Hybridization bandgap induced by an electrical resonance in piezoelectric metamaterial plates

Nesrine Kherraz, Lionel Haumesser, Franck Levassort, P. Benard, B. Morvan

Hybridization bandgap induced by an electrical resonance in piezoelectric metamaterial plates

N. Kherraz, L. Haumesser, F. Levassort, P. Benard, and B. Morvan

Citation: Journal of Applied Physics **123**, 094901 (2018); doi: 10.1063/1.5016496
View online: https://doi.org/10.1063/1.5016496
View Table of Contents: http://aip.scitation.org/toc/jap/123/9
Published by the American Institute of Physics

Hybridization bandgap induced by an electrical resonance in piezoelectric metamaterial plates

N. Kherraz,[1,2,3] L. Haumesser,[2] F. Levassort,[2] P. Benard,[1] and B. Morvan[1]
[1]*University of Normandie, UNIHAVRE, Laboratoire Ondes et Milieux Complexes, UMR CNRS 6294, 75 Rue Bellot, 76600 Le Havre, France*
[2]*University of Tours, GREMAN, UMR CNRS 7347, 03 Rue de la Chocolaterie, 41000 Blois, France*
[3]*Department of Physics, University of Torino, Via Pietro Giuria 1, 10125 Torino, Italy*

(Received 20 November 2017; accepted 20 February 2018; published online 5 March 2018)

We demonstrate numerically and experimentally the opening of a locally resonant bandgap in an active phononic crystal (PC) made of a homogeneous piezoelectric plate covered by a 1D periodic array of thin electrodes connected to inductive shunts. The application of periodic electrical boundary conditions (EBCs) enables an at will tailoring of the dispersion properties of the PC plate, thus leading to a control of the dispersion of the propagating guided elastic waves in the plate. Depending on the nature of the EBCs, several bandgaps open up, the most important being a Hybridization Bandgap (HBG) in the subwavelength regime. The PC behaves as a locally resonant metamaterial. The HBG originates from the interaction of propagating elastic waves (Lamb modes) with an electrical resonant mode whose dispersion can be effectively described through an equivalent transmission line model. *Published by AIP Publishing.*
https://doi.org/10.1063/1.5016496

I. INTRODUCTION

During the last few years, phononic crystals (PCs) have demonstrated their great ability to manipulate elastic waves. Selective filtering,[1] beamforming,[2] super resolution imaging,[3] and acoustic resonators[4] are, among many others, different applications that have emerged. Phononic crystals derive their properties from the periodic arrangement of their constitutive materials. This periodicity has to be of the order of the wavelength of the propagating waves, which explains why most of the experiments and practical applications have been developed for ultrasonic waves for which the wavelength remains small. Recently, the willingness to reduce the size and weight of devices, for instance, for the audible sound mitigation purpose or for electronic applications where miniaturization is needed, has led to a strong interest in locally resonant metamaterials (MMs) that enable the control of wave propagation at deep sub-wavelength scale. One way to achieve a locally resonant material is to use the high sound velocity contrast between the host matrix material and embedded inclusions. Using metallic spheres coated with silicone in an epoxy matrix, Liu *et al.* developed a sonic MM with bandgap caused by negative effective elastic constants with a lattice constant 300 times smaller than the wavelength in epoxy.[5] Brunet *et al.*[6] exploited Mie resonances of soft porous silicone rubber particles together with their surrounding fluid matrix to obtain a metafluid, exhibiting simultaneously negative effective mass density and bulk modulus. However, this MM is difficult to use in practice for the realization of a super-resolution lens due to strong absorption inside the porous inclusions.

The use of active materials such as piezoelectric materials is another way to obtain local resonances within a MM. Such mechanisms that couple mechanical vibrations to electrical passive or active circuits have been extensively studied in the low frequency range for their ability in vibration damping and energy harvesting.[7–13] In addition, the insertion of piezoelectric materials in PCs offers a frequency agility which can be easily controlled electrically and does not require any geometry modification nor phase transition of constitutive materials.[8–10,13–15] For instance, a Bragg gap can be shifted by switching from the open to the short circuit the electrical boundary condition (EBC) of piezoelectric inclusions in a PC.[16] Electrical resonances can be easily induced in a piezoelectric element by connecting an inductive shunt. Several studies aim at the attenuation of structure vibrations by sticking piezoelectric elements linked to an independent inductive circuit. It was demonstrated theoretically and experimentally that these structures exhibit hybridization bandgaps (HBGs) at the electrical resonance frequencies.[17–21] This technique gives the opportunity to tune the stiffness of the substrate as reported by Bergamini *et al.*[22] and to modify the wave dispersion in the medium by tailoring the external electrical circuit. In their work, piezoelectric discs are inserted between an aluminium substrate, where guided waves propagate, and cylindrical stubs arranged periodically on the surface. The implementation of this kind of EBC is simple and can also be efficient at high frequencies by implementing active circuits. However, these resonators are isolated between each other and have inherently narrow frequency band behavior, thus limiting the coupling with the mechanical modes supported by the waveguide. To overcome this limitation, some authors have proposed a hybrid electric/mechanical medium:[23–27] the spatial periodicity of the mechanical part is settled by the arrangement of the piezoelectric elements, whereas the electrical part is composed of the lumped transmission line achieved by combining inductive circuits with resistors and the piezoelectric elements. This enables the propagation of

energy in both the electrical line and the plate. Finally, the interaction between the electrical and the mechanical modes induces a locally resonance bandgap and allows us to improve considerably the control performances of this class of electro-mechanical structures.[28,29]

In this paper, we consider an electro-mechanical phononic crystal made of a homogeneous piezoelectric plate covered by a 1D periodic array of thin electrodes.[30] The control of the propagating elastic guided wave is achieved by connecting inductive loads to the electrodes array. The application of these EBCs at the piezoelectric plate generates local resonances periodically distributed along the waveguide, giving rise to a dispersive electrical mode. A hybridization bandgap (HBG) originating from the coupling of this dispersive electrical mode with the guided Lamb waves inside the piezoelectric metamaterial plate is investigated numerically and experimentally.

II. STRUCTURE PRESENTATION

We shall be concerned, in this study, with a piezoelectric homogeneous plate polarized across its thickness h and covered with a periodic array of conductive electrodes. In the calculations, the electrodes are modeled as perfectly conductive surfaces whose thickness will be neglected and the mechanical effect due to added mass. For the experiments, a PZT (Pz26[31]) finite square plate (80 mm × 80 mm) with thickness $h = 2.2$ mm was used. Two silver electrodes on both sides were deposited by screen-printing on the full area with a thickness of around 15 μm. Forty periodic rectangular electrodes on each face were designed using a dicing saw to remove the conductive material as schematically illustrated in Fig. 1(a). Particular attention was paid to deliver face-to-face electrodes on each side of the plate during this machining step. The width of each electrode is measured to be $a = 1.7$ mm, and the spacing between two neighboring electrodes is $b = 0.3$ mm. We will adopt the same values for the numerical calculations as well.

The inherent electro-mechanical coupling of the piezoelectric plate allows us to determine the effective elastic properties of the plate by changing the electric boundary conditions. By this way, it is possible to control the propagation of the elastic guided waves in the plate. In choosing different EBCs in adjacent electrodes, one can expand the unit cell length from $\Lambda = a + b$ to $\Lambda' = 2\Lambda$ [see Figs. 1(a), 1(b), 1(c), and 1(d)]. Different electrical boundary conditions will be considered, particularly the case of a connected inductor load on the electrodes.

III. RESULTS AND DISCUSSION

A. Band structure calculations

To begin with, we perform 2D finite element calculations (we use the commercial software COMSOL *Multiphysics*) to obtain the frequency band structure of the PC plate described previously. An infinite plate (xy-plane with the electrodes oriented along the y-axis) is considered, and the Bloch-Floquet theorem is applied to compute the wave dispersion. With the plate being piezoelectric, enabling

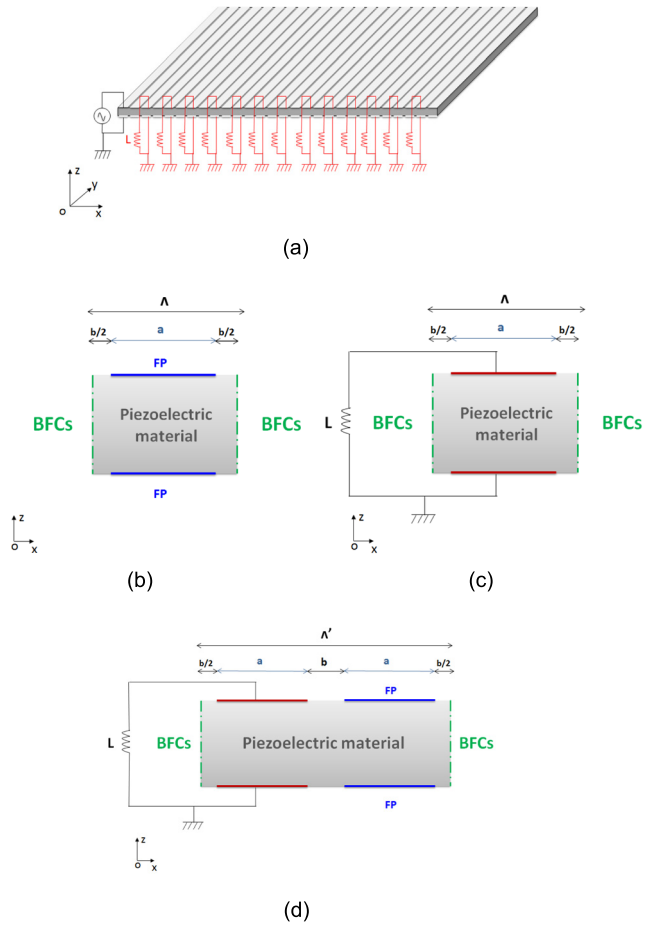

FIG. 1. (a) Schematic representation of the piezoelectric phononic plate of thickness h with a set of periodic electrode segments (electrode width $a = 1.7$ mm and separation distance $b = 0.3$ mm) on both faces. Different EBC configurations defining the representative unit cell of the periodic structure (lattice constant Λ): (b) electrodes in floating potential ($\Lambda = 2$ mm), (c) inductance load L connected to each pair of electrodes ($\Lambda = 2$ mm), and (d) electrodes having alternatively a FP and an inductance load L ($\Lambda' = 4$ mm). Bloch-Floquet conditions (BFCs) are applied at the boundaries denoted by dash-dotted lines.

coupling of mechanical and electrical fields, periodic boundary conditions have to be applied for both the displacements $u(x + \Lambda, k_x) = u(x, k_x)e^{-ik_x\Lambda}$ and the electrical potentials $V(x + \Lambda, k_x) = V(x, k_x)e^{-ik_x\Lambda}$ at the unit cell boundaries (see Fig. 1). In these expressions, k_x is the wavenumber along the x direction of propagation.

The parameters used in the calculations can be found in Ref. 31. An eigenvalue study is performed to evaluate the band structure of Lamb-like modes along the highest symmetry $\Gamma - X$ line of the Brillouin zone (BZ). Frequencies of the propagating waves are then deduced for each real value of the wavevector k_x lying in the half first BZ $[0, \pi/\Lambda]$.

First, the dispersion curves are computed in the case where all the electrodes have a floating potential (FP) as illustrated in Fig. 1(b). The band structure presented in Fig. 2(a) shows the folded dispersion curves of the first three guided Lamb modes A_0, S_0, and A_1. A and S denote waves with antisymmetric motion and symmetric motion, respectively, with respect to the middle plane of the plate.[32] From a practical point of view, the excitation of A and S waves therefore depends on the symmetry of the electrical potential

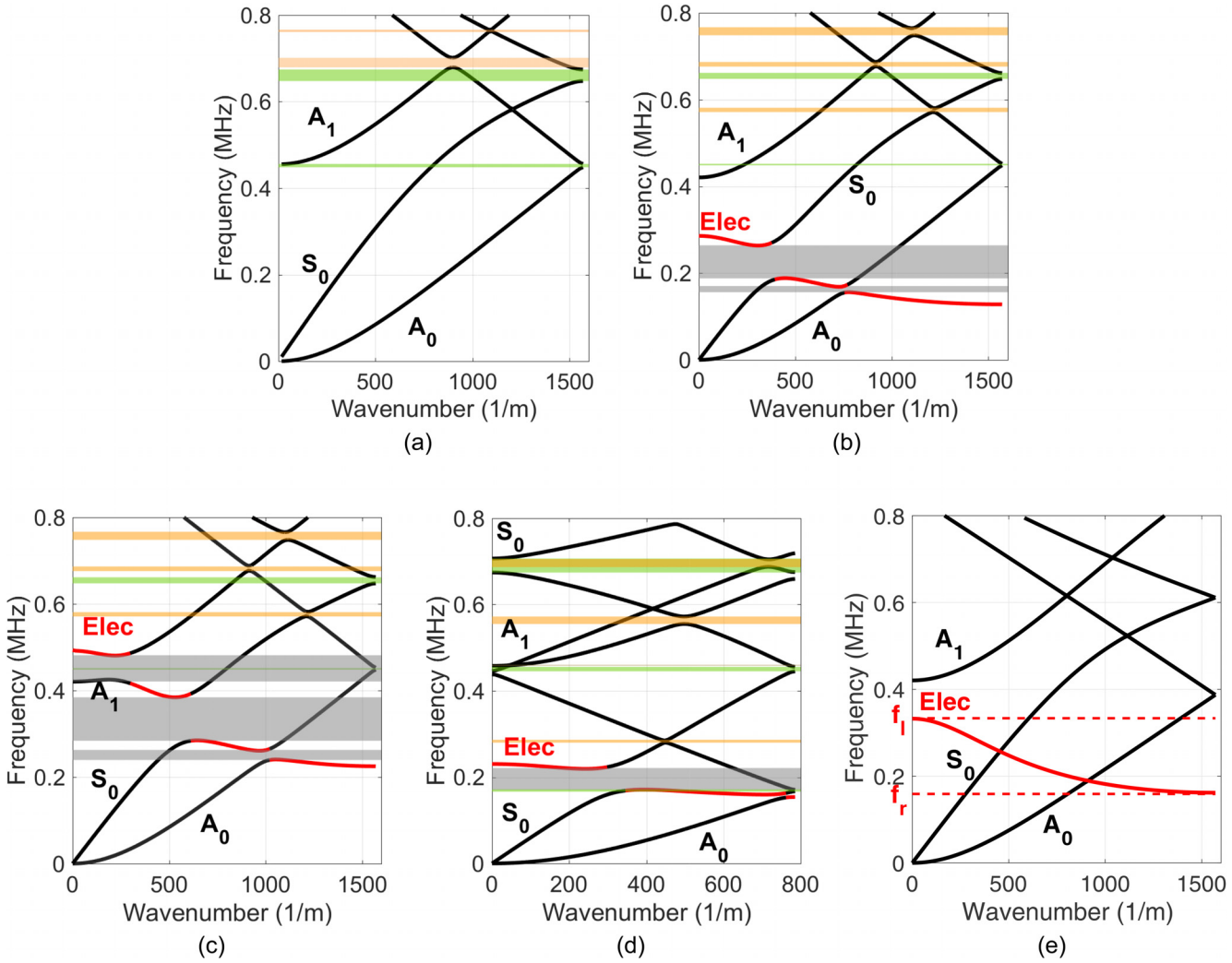

FIG. 2. Dispersion curves of the infinite phononic piezoelectric plate (a) with electrodes having floating potential (unit cell length $\Lambda = 2$ mm), (b) with electrodes connected to inductors $L_1 = 470\,\mu$H (unit cell length $\Lambda = 2$ mm), (c) with electrodes connected to inductors $L_2 = 150\,\mu$H (unit cell length $\Lambda = 2$ mm), and (d) with electrodes connected alternatively to inductors $L_1 = 470\,\mu$H and having a FP (unit cell length $\Lambda' = 4$ mm). (e) The same as (b) but without piezoelectric effects. The green, orange, and gray areas indicate the Bragg BGs at the edge of the Brillouin zone, avoided-crossing BGs in the middle of the Brillouin zone, and locally resonant BGs, respectively. The electrical mode (Elec) is represented in red and is generated between the frequencies f_r and f_l.

applied on the plate. In addition, some mode conversions could exist between symmetric and asymmetric modes if asymmetric (mechanical or electrical) boundary conditions with respect to the median plane of the plate are applied on the plate. Several bandgaps (BGs) are also observed. These bandgaps (BGs) originate from interference mechanisms involving one mode (at the edge of the BZ) or two different modes (inside the BZ). The green-shaded areas indicate the BG involving the A_0 modes, at about 450 kHz, or S_0 modes at about 660 kHz. These gaps are achieved by the periodicity of the electrical boundary conditions, leading to periodic variations of the effective elastic properties of the piezoelectric medium.[30] The other two, orange-shaded, areas in this plot indicate a coupling between two different Lamb modes, leading to the opening of partial bandgaps. The coupled modes are counter-propagating, and as described by Mace and Manconi, this leads to a locking of the dispersion curves.[33] The strength of these couplings depends on the EBC symmetry of the unit cell with respect to the middle plane of the plate. Here, the symmetry of the EBCs favors the interaction between modes having the same symmetry (see the coupling between A_0 and A_1 at about 690 kHz).

Next, an inductance load L is connected between the two electrodes of the unit cell [Fig. 1(c)]. The shunt circuit is implemented using the *Global ODEs and DAEs* interface of COMSOL *Multiphysics*. A charge q is defined on the top electrode of the unit cell, while the bottom electrode is grounded. The charge q is linked to the voltage U_p between the electrodes following the Kirchhoff voltage law

$$U_p - L\omega^2 q = 0, \tag{1}$$

with ω the angular frequency. Finally, an eigenvalue analysis is performed to evaluate the band structure. We compute the dispersion curves for two different values of the inductor ($L_1 = 470\,\mu$H, $L_2 = 150\,\mu$H). The resulting band structures are plotted in Fig. 2(b). The Bragg bandgaps of the S_0 and A_0 modes at the edge of the Brillouin zone are still open (green areas). In this case, the asymmetry of the EBCs driven by the grounded electrodes favors the coupling between modes

with different symmetries. It is clear from Fig. 2(b) that the opening of the gap resulting from the coupling of A_0 and S_0 modes and S_0 and A_1 modes has increased to reach relative widths of 1.6% and 2.5%, respectively, while that of A_0 and A_1 coupling has decreased to 1.5%.

In addition to these slight bandgap modifications, a supplementary dispersion curve is observed. In the first case ($L_1 = 470\,\mu$H), the supplementary mode is present between 128 kHz and 286 kHz [see Fig. 2(b), red lines] and is strongly coupled to the S_0 mode, leading to the opening of an avoided-crossing gap between 188 kHz and 264 kHz (indicated with the gray area). The coupling with the fundamental A_0 mode is weaker, but a small bandgap between 156 kHz and 170 kHz is also observed (gray area). As it is well-known, a piezoelectric plate electrically behaves like a capacitor C; by adding an inductance load L, we obtain an electrical resonant circuit LC. Contrary to previous studied metamaterials,[26] the supplementary branch, originating from the presence of electrical resonances LC, spreads over a large frequency range and is not only localized around the typical resonance frequency $f_0 = 1/2\pi\sqrt{LC}$. The term "Electric mode" used in Fig. 2 refers to the physical phenomenon underlying the presence of this supplementary mode. As already described by Bergamini *et al.*,[26] the associated electric field across the thickness of the plate is uniform contrarily to the electric field induced by the propagation of the Lamb modes in the piezoelectric plate. This distinctive feature is used to identify the part of the dispersion curves associated with the electric mode (see the red line in Fig. 2).

It is worth noting that the bandgap originating from the coupling between the electrical resonance and the S_0 mode opens up at $f = 200$ kHz corresponding to a wavelength $\lambda \sim 10\Lambda$. The mechanism leading to this forbidden band is no more linked to the periodicity of the PC but only to the hybridization between the electrical resonance and the guided Lamb mode. The former can be easily tuned by changing the value of the inductor, as confirmed in Fig. 2(c). For $L_2 = 150\,\mu$H, the electrical mode is now shifted toward higher frequencies (between 225 kHz and 493 kHz), thus inducing a HBG with the S_0 mode at also higher frequencies. Moreover, a supplementary HBG opens up involving the A_1 mode. Of course, an increase in the inductor value will shift the HBG toward the lower frequency range.

We close this section by the case of an expanded unit cell including two adjacent pairs of electrodes ($\Lambda' = 4$ mm) in order to study how this affects the electrical mode. We compute the band structure of a piezoelectric PC plate having alternatively the first pair of electrodes in FP and the second one connected to an inductor $L = 470\,\mu$H [see Fig. 1(c)]. The results shown in Fig. 2(d) point out that even if the Bragg bandgaps are shifted toward lower frequencies (green areas), the electrical mode and the relating HBGs are still generated at the same frequency position as for the case of the simplest unit cell ($\Lambda = 2$ mm).

B. Electrical line model

In order to further investigate the dispersive electrical mode, the dispersion curves of the PC under study are computed numerically by canceling the piezoelectric coupling coefficients. Electrical and mechanical modes are now decoupled, and all frequency bandgaps are closed as shown in Fig. 2(e). Indeed, the periodicity in the PC is only introduced via the electric boundary conditions, and if the piezoelectric coupling is suppressed, then mechanical waves propagate in a homogeneous plate without any discontinuity in the x direction. The folding of the dispersion curves is due to the fact that the numerical computation is performed on a unit cell of length Λ. The dispersion of the electrical mode still exists, and this mode covers a frequency range which extends from f_r to f_l. In Fig. 2(b), the supplementary electrical mode is coupled with the classical Lamb type modes, leading to the opening of a gap in the band structure. Of course, this coupling affects the dispersion of both the electrical and mechanical modes involved, and therefore, considering piezoelectric effects, the cut-off frequencies f_r and f_l are shifted. The proposed transmission line model does not take into account the mode coupling and is therefore related to the case without the piezoelectric effect [Fig. 2(e)]. This dispersive cos-like resonance band can be reproduced by making use of a simple transmission line model, describing effectively the behavior of the PC, as shown in Fig. 3. Each piezoelectric unit cell is represented by a capacitor C connected in parallel to an inductor L. The electrical coupling between two adjacent electrodes is modeled by a shunt capacitor C'.

The potential difference between the cell N and its nearest neighbors $(N-1)$ and $(N+1)$ can be written as follows:

$$\frac{1}{jC'\omega} I_e = V_{N-1} - V_N, \tag{2a}$$

$$\frac{1}{jC'\omega} I_s = V_N - V_{N+1}, \tag{2b}$$

where I_e et I_s are the inward and outward current, respectively, at the cell N,

$$I_p = I_e - I_s. \tag{3}$$

In the cell N, the ratio of the voltage V_N and the current I_p is given by the characteristic impedance Z_{eq},

$$\frac{V_N}{I_p} = Z_{eq}, \tag{4}$$

with

$$Z_{eq} = \left[\frac{1}{jL\omega} + jC\omega\right]^{-1}. \tag{5}$$

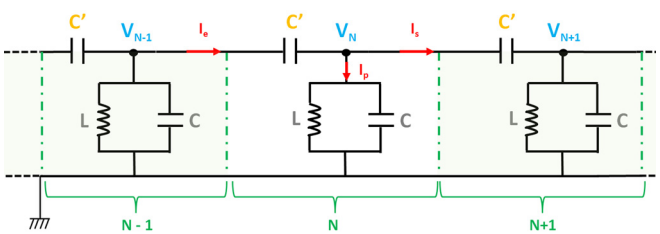

FIG. 3. Equivalent electrical diagram of the transmission line. The unit cell N is composed of capacitors C and C' and inductor L.

Electrical potentials must satisfy the Bloch-Floquet conditions

$$V_{N-1} = V_N e^{jk\Lambda}, \tag{6a}$$

$$V_{N+1} = V_N e^{-jk\Lambda}. \tag{6b}$$

Substituting Eq. (6) into Eq. (2), we find the dispersion relation for the electrical mode to be

$$\frac{k\Lambda}{2\pi} = \frac{1}{\pi}\arcsin\left(\frac{1}{2}\sqrt{\frac{1}{LC'\omega^2} - \frac{C}{C'}}\right). \tag{7}$$

The study of the two extreme cases corresponding to short ($k\Lambda/2\pi = 1/2$, $\lambda = 2\pi/k = 2\Lambda$) and long ($k\Lambda/2\pi = 0$, $\lambda \gg \Lambda$) wavelengths can shed light to the dispersion of the electrical mode described by Eq. (7). First [Fig. 4(a)], the electrical charges of two adjacent electrodes are equal, and the capacitor C' can thus be neglected. The dispersion relation gives the cut-off frequency f_l,

$$f_l = \frac{1}{2\pi\sqrt{LC}} = f_0. \tag{8}$$

As displayed in Fig. 4(a), the electrical mode is only fixed by the capacitance of the piezoelectric element C corresponding to the capacitor between the two electrodes of the unit cell and the inductor L. The frequency of the line corresponds to the resonance frequency of the LC circuit.

When the wavenumber is close to π/Λ, at the limit of the BZ, $\lambda = 2\Lambda$, and there is a succession of positive and negative charges on electrodes as shown in Fig. 4(b). The effect of the capacitor C' becomes important, and the cut-off frequency of the mode is

$$f_r = \frac{1}{2\pi}\sqrt{\frac{1}{L(4C'+C)}} = f_0\sqrt{\frac{1}{4C'/C+1}}. \tag{9}$$

From the cut-off frequencies $f_r = 161.8\,\text{kHz}$ and $f_l = 332.4\,\text{kHz}$ in Fig. 2(e), the values of the capacitor $C' = 0.39\,\text{nF}$ and $C = 0.48\,\text{nF}$ are deduced, and the dispersion relation (7) provides the real and imaginary parts of the wavenumber plotted in Fig. 5.

The electrical mode originates from the electric resonance of the interaction between the capacitor C between two face-to-face electrodes and the inductors, but the dispersion relation describing this mode takes into account the coupling between adjacent electrodes, effectively described by

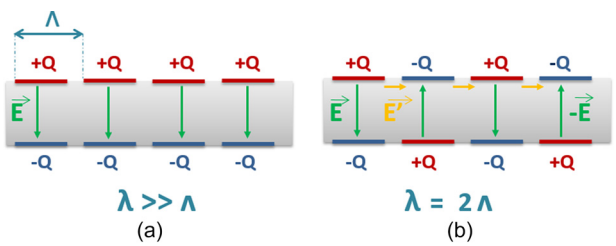

FIG. 4. Direction of the electrical field within the phononic piezoelectric plate in the cases of (a) $\lambda \gg \Lambda$ and (b) $\lambda = 2\Lambda$.

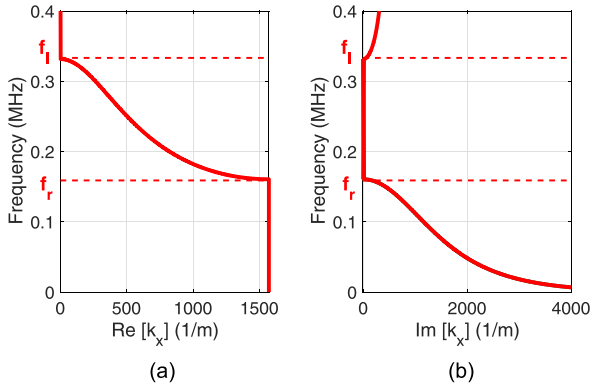

FIG. 5. Dispersion curves computed from the line transmission model. The frequency is represented as a function of (a) the real and (b) the imaginary part of the wavenumber.

the capacitor C'. Moreover, the variation of C' with the separation distance between two electrodes b presented in Fig. 6 points out that, as expected, the smaller the spacing between adjacent electrodes, the stronger the C' (the interaction between unit cells becomes more important), and inversely, C' becomes negligible for long separation distances. The results shown in Fig. 6 are obtained by computing the numerical dispersion curves of the PC structures without piezoelectric coupling [as in Fig. 2(e)], with the width of each electrode kept at $a = 1.7\,\text{mm}$, for different values of the parameter b ranging from 0.1 mm to 50 mm. From each dispersion curve, we evaluate the edge frequencies f_r and f_l that we use in Eqs. (8) and (9) to obtain C'.

C. Experimental results

Scanning Laser Doppler Vibrometer measurements are performed in order to validate the numerically predicted S_0 HBG. A waveform generator is used to deliver a 10V electrical tune burst (5 periods) centered at the frequency of 200 kHz. The electrical signal is applied to the first couple of electrodes located at the edge of the plate. Due to the symmetric excitation, we expect to generate mainly symmetric

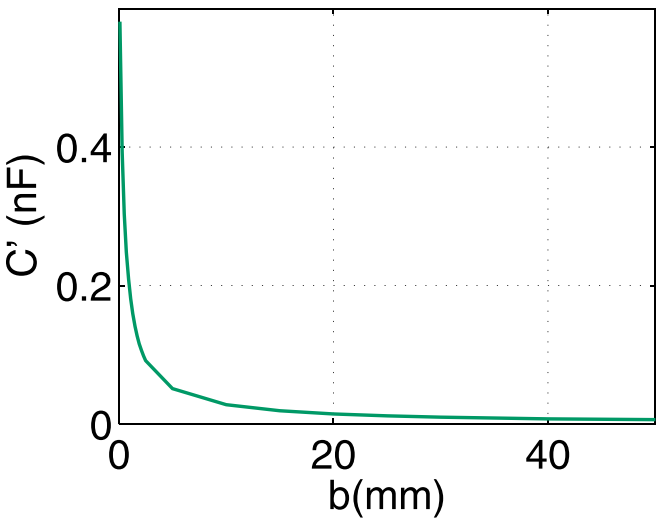

FIG. 6. Variation of capacitor C' as a function of separation distance b between two electrodes for a fixed width of electrodes $a = 1.7\,\text{mm}$.

Lamb modes. The 1D scan using a Polytec laser vibrometer is conducted along the x-direction of propagating Lamb waves with a spatial resolution of 0.1 mm. At each position, the signal is averaged 512 times to improve the signal-to-noise ratio. The spatio-temporal signals obtained are then windowed to remove the part corresponding to the reflected waves arising from the end of the plate. Finally, temporal and spatial Fourier transforms (FFTs) are successively applied to the data to obtain the experimental dispersion curves.

In order to observe the coupling of the electrical wave with the propagating elastic waves and particularly with the S_0 Lamb mode as described in Sec. II, two configurations are considered. The first one consists of electrodes with a floating potential (open circuit). The unit cell is made of one pair of electrodes and has a length equal to Λ as illustrated in Fig. 1(b). The resulting experimental dispersion curves are plotted at a color level in Fig. 7 with numerically predicted curves superimposed for a sake of comparison [Fig. 7(a)]. We observe the generation of the S_0 wave around 200 kHz without any conversion or reflection during the propagation as illustrated in Fig. 7(b) where no signal is present in the half-space of negative wavenumbers. The second configuration described in Fig. 1(d) with a unit cell size equal to $\Lambda' = 2\Lambda$ and an electrode over two connected to an inductor.

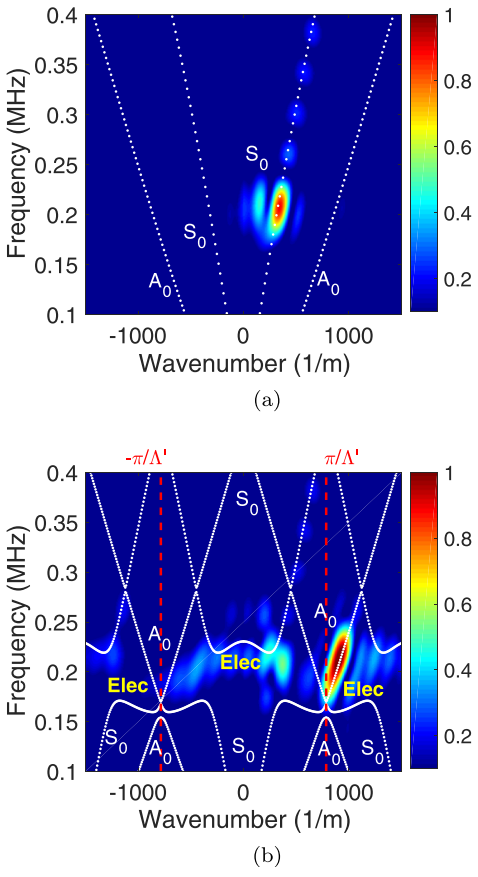

FIG. 7. Fourier transform modulus of the measured spatio-temporal signals for (a) all electrodes having a floating potential and (b) one couple of electrodes over two connected to inductor $L = 470\,\mu$H and the others having a floating potential. The color map represents the amplitudes of the 2D Fourier transform modulus, and the white curves represent the numerical predictions. The first Brillouin zone is delimited by dotted red lines.

Our measurements confirm in this case a significant attenuation of the S_0 mode, and the spot previously observed in the theoretical S_0 dispersion curve has almost completely disappeared in the frequency range lying within the HBG. Most of the input energy is now converted into the A_0 mode [see Fig. 7(b)] which is the only propagating mode present at this frequency. These results clearly illustrate the coupling of the electrical wave with the propagating elastic waves guided in the plate and the efficiency of the HBG to stop the propagation of the guided S_0 waves.

A quantitative estimation of the attenuation can be done by evaluating the ratio $\alpha(f)$ of the amplitude of the S_0 wave in the PC without inductive shunt, $A_{FP}^{S_0}(f)$, over the amplitude of the S_0 wave in the PC with the inductive shunt, $A_L^{S_0}(f)$ [Eq. (10)]. In order to observe a significant effect of the HBG, the amplitudes are evaluated after a distance of propagation corresponding to 5 periods of the PC,

$$\alpha(f) = 20\log\left(\frac{A_{FP}^{S_0}(f)}{A_L^{S_0}(f)}\right). \tag{10}$$

Amplitudes are extracted from 2D FFT performed on the spatio-temporal signals acquired along the propagation direction between $x = 20$ mm and $x = 60$ mm ($x = 0$ mm is related to the first edge of the plate where waves are excited).

Figure 8 shows that the attenuation reaches a maximum value of 50 dB around 200 kHz, which is located at the middle of the HBG. It can be observed that the attenuation measured in the close neighborhood of the bandgap remains significant. This can be explained on the one hand by the fact that the theoretical width of the bandgap is computed for an infinite extended PC, while experiments are performed on a finite one. It is well known that this leads to a widening of the BG frequency range.[32] On the other hand, the width and the position of the HBG are strongly affected by the values of the connected inductance L and capacitance C associated with each element (unit cell) of the PC. There is a slight dispersion of the inductance values L used in experiments, and the values of the capacitance C near the edges of the plate differ from those measured in the middle of the plate. This explains why the experimental attenuation is observed in a wide frequency range greater than the theoretical width of the HBG.

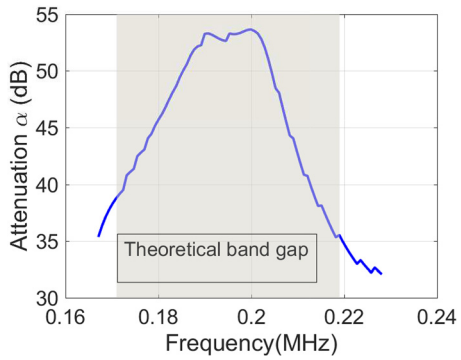

FIG. 8. Experimental attenuation coefficient as a function of frequency. The numerically computed bandgap is shown in the gray-shaded region.

IV. CONCLUSION

The piezoelectric metamaterial studied in this paper shows not only classical properties linked to the periodicity of the distributed electrodes on the plate, e.g., opening of Bragg gaps at the limit of the Brillouin zone and coupling of Lamb guided waves inside the BZ, but also more importantly opening of HBG easily tuned electrically through a change of inductor connected loads on the electrodes. The electrical dispersive mode induced by the presence of the inductance loads has been studied through a model of the electrical transmission line. It is shown that the dispersive properties of this mode are, as expected, related to the inductor value and also depend on the size and the way the conductive electrodes are distributed along the plate. The HBG induced by the coupling between the fundamental symmetrical S_0 mode with the electrical mode opens up at a sub-wavelength scale, with the lattice constant of the periodic array of electrodes being more than ten times the wavelength of the wave. The proposed active device opens up many perspectives, for instance, with the use of active circuits to control the electrical boundary conditions on the metamaterial. The implementation of dynamic loads could also offer some new applications in the field of wave propagation control.

ACKNOWLEDGMENTS

We gratefully acknowledge Christophe Brosseau (Blois Institute of Technology) for sample preparation. This work is supported by the French National Research Agency (project MIRAGES ANR-12-BS09-0015) and by the Acoustic Federation of the North-West (FANO FR CNRS 3110). The authors acknowledge support for this work from the project "Metapp" (n. CSTO160004) cofunded by Fondazione San Paolo.

[1]A. Khelif, P. Deymier, B. Djafari-Rouhani, J. Vasseur, and L. Dobrzynski, J. Appl. Phys. **94**, 1308 (2003).
[2]S. Yang, J. Page, Z. Liu, M. Cowan, C. Chan, and P. Sheng, Phys. Rev. Lett. **93**, 024301 (2004).
[3]A. Sukhovich, B. Merheb, K. Muralidharan, J. Vasseur, Y. Pennec, P. Deymier, and J. Page, Phys. Rev. Lett. **102**, 154301 (2009).
[4]S. Mohammadi, A. A. Eftekhar, W. D. Hunt, and A. Adibi, Appl. Phys. Lett. **94**, 051906 (2009).
[5]Z. Liu, X. Zhang, Y. Mao, Y. Zhu, Z. Yang, C. Chan, and P. Sheng, Science **289**, 1734 (2000).
[6]T. Brunet, A. Merlin, B. Mascaro, K. Zimny, J. Leng, O. Poncelet, C. Aristégui, and O. Mondain-Monval, Nat. Mater. **14**, 384 (2015).
[7]N. W. Hagood and A. von Flotow, J. Sound Vib. **146**, 243 (1991).
[8]A. Baz, J. Vib. Acoust. **123**, 472 (2001).
[9]C. Sheng-Bing, W. Ji-Hong, Y. Dian-Long, W. Gang, and W. Xi-Sen, Chin. Phys. B **20**, 014301 (2011).
[10]Y. Chen, G. Huang, and C. Sun, J. Vib. Acoust. **136**, 061008 (2014).
[11]S. Gonella, A. C. To, and W. K. Liu, J. Mech. Phys. Solids **57**, 621 (2009).
[12]Z. Chen, Y. Yang, Z. Lu, and Y. Luo, Phys. B: Condens. Matter **410**, 5 (2013).
[13]S. Degraeve, C. Granger, B. Dubus, J.-O. Vasseur, M. P. Thi, and A.-C. Hladky-Hennion, J. Appl. Phys. **115**, 194508 (2014).
[14]M.-F. Ponge, B. Dubus, C. Granger, J. Vasseur, M. P. Thi, and A.-C. Hladky-Hennion, Phys. Procedia **70**, 258 (2015).
[15]A. Kutsenko, A. Shuvalov, O. Poncelet, and A. Darinskii, J. Acoust. Soc. Am. **137**, 606 (2015).
[16]C. Croënne, M.-F. Ponge, B. Dubus, C. Granger, L. Haumesser, F. Levassort, J. O. Vasseur, A. Lordereau, M. Pham Thi, and A.-C. Hladky-Hennion, J. Acoust. Soc. Am. **139**, 3296 (2016).
[17]O. Thorp, M. Ruzzene, and A. Baz, Smart Mater. Struct. **10**, 979 (2001).
[18]A. Spadoni, M. Ruzzene, and K. Cunefare, J. Intell. Mater. Syst. Struct. **20**, 979 (2009).
[19]L. Airoldi and M. Ruzzene, New J. Phys. **13**, 113010 (2011).
[20]F. Casadei, T. Delpero, A. Bergamini, P. Ermanni, and M. Ruzzene, J. Appl. Phys. **112**, 064902 (2012).
[21]H. Zhang, J. Wen, Y. Xiao, G. Wang, and X. Wen, J. Sound Vib. **343**, 104 (2015).
[22]A. Bergamini, T. Delpero, L. D. Simoni, L. D. Lillo, M. Ruzzene, and P. Ermanni, Adv. Mater. **26**, 1343 (2014).
[23]S. Vidoli and F. Dell'Isola, Acta Mech. **141**, 37 (2000).
[24]F. dellIsola, C. Maurini, and M. Porfiri, Smart Mater. Struct. **13**, 299 (2004).
[25]C. Maurini, F. Dell'Isola, and D. Del Vescovo, Mech. Syst. Signal Process. **18**, 1243 (2004).
[26]A. E. Bergamini, M. Zündel, E. A. F. Parra, T. Delpero, M. Ruzzene, and P. Ermanni, J. Appl. Phys. **118**, 154310 (2015).
[27]E. A. Flores Parra, A. Bergamini, B. Van Damme, and P. Ermanni, Appl. Phys. Lett. **110**, 184103 (2017).
[28]C. Sugino, S. Leadenham, M. Ruzzene, and A. Erturk, Smart Mater. Struct. **26**, 055029 (2017).
[29]E. A. Flores Parra, A. Bergamini, B. Lossouarn, B. Van Damme, M. Cenedese, and P. Ermanni, Appl. Phys. Lett. **111**, 111902 (2017).
[30]N. Kherraz, L. Haumesser, F. Levassort, P. Benard, and B. Morvan, Appl. Phys. Lett. **108**, 093503 (2016).
[31]See http://www.ferroperm-piezo.com for the properties of the piezoelectric materials.
[32]M. Bavencoffe, A.-c. Hladky-Hennion, B. Morvan, and J.-l. Izbicki, IEEE Trans. Ultrason., Ferroelectr., Freq. Control **56**, 1960 (2009).
[33]B. R. Mace and E. Manconi, J. Acoust. Soc. Am. **131**, 1015 (2012).